Research Article | Vol. 12, No. 1 / 1 January 2021 / Biomedical Optics Express 320
Biomedical Optics EXPRESS

Direct measurement of the scattering coefficient

MARTIN HOHMANN,[1,2,*] BENJAMIN LENGENFELDER,[1,2] DANIEL MUHR,[1] MORITZ SPÄTH,[1,2] MAXIMILIAN HAUPTKORN,[1] FLORIAN KLÄMPFL,[1,2] AND MICHAEL SCHMIDT[1,2]

[1] *Institute of Photonic Technologies (LPT), Friedrich-Alexander-Universität Erlangen-Nürnberg (FAU), Germany*
[2] *Erlangen Graduate School in Advanced Optical Technologies (SAOT), Paul-Gordan-Straße 6, 91052 Erlangen, Germany*
[*] *Martin.Hohmann@FAU.de*

Abstract: In general, the measurement of the main three optical properties (μ_a, μ_s and g) in turbid media requires a very precise measurement of the total transmission (TT), the total reflection (TR) and the collimated transmission (CT). Furthermore, an inverse algorithm such as inverse adding doubling or inverse Monte-Carlo-simulations is required for the reconstruction of the optical properties. Despite many available methods, the error free measurement of the scattering coefficient or the g-factor still remains challenging. In this study, we present a way to directly calculate the scattering coefficient from the total and collimated transmission. To allow this, it can be shown that $\frac{TT}{CT}$ is proportional to $e^{\mu_s \cdot d}$ for a wide range of optical properties if the sample is thick enough. Moreover, a set-up is developed and validated to measure the collimated transmission precisely.

1. Introduction

Determining the propagation of light through biological tissues is crucial for many medical diagnostics and therapies such as the photodynamic therapy (PDT) [1,2]. Moreover, it has been evaluated for potential cancer detection [3,4]. Reports show that in a certain wavelength range, differences in the scattering coefficient appear between healthy and cancerous human skin which may form a reliable base for pathology discrimination [3]. To ensure correct treatments and diagnostics within these applications, the distribution of light within the tissue needs to be accurately determined. Light propagation through tissue can be calculated if the optical properties of the tissue are known, namely the absorption coefficient μ_a, the scattering coefficient μ_s and the anisotropy factor g. Measurements of the optical properties are, therefore, an essential part of determining light propagation. Several techniques have been developed and evaluated to estimate the optical properties of biological tissue ex vivo as well as in vivo. Considering the ex vivo techniques, two different kind of measurements can be defined: direct and indirect measurements.

Within direct measurements a macroscopic quantity such as the collimated transmission (CT) is measured. Moreover, no light propagation model is assumed. The optical properties are accessed by directly measuring microscopic parameters using thin tissue samples where multiple scattering can be neglected [5]. From measurements of the CT, by simple narrow beam transmission geometries, the total attenuation coefficient μ_t can be obtained [5]. CT can be measured by polarized input beam and polarization filtered measurement of the transmission. For unpolarized light as only unscattered photons, from the strongly forward scattering light of biological tissue, should be detected the beam needs to be very collimated. Measuring all photons transmitted, or reflected provides access to the absorption coefficient μ_a and reduced scattering coefficient μ_s'. This can be done with integrating sphere measurements.

#410248 https://doi.org/10.1364/BOE.410248
Journal © 2021 Received 15 Sep 2020; revised 23 Nov 2020; accepted 23 Nov 2020; published 14 Dec 2020

Biomedical Optics EXPRESS

Within integrating sphere measurements light losses have a significant effect on the estimation of the optical properties as they lead to an overestimation of the absorption coefficient [6]. In an integrating sphere set-up the main leaking components are the entrance port [7] and glass slides used to hold the sample in place where multiple internal reflections can occur [6].

With goniometric techniques, where a detector is moved radially around the sample, the scattering phase function can be measured which can be used to calculate the g-factor. Biological tissue has shown a strongly forward scattering behaviour [8]. Therefore at larger angles from the forward direction, the detected signal is very low compared to the intensity of the incident light. To avoid disturbance from any other light sources any background effects need to be reduced [5]. As thin samples are required for direct measurements, problems may arise in preparing and handling the samples. For example due to dehydration altering the optical properties [9], the results might be influenced. Moreover, signals obtained from thin samples are comparable weak compared to the incident light. Hence, background effects likely lead to errors [5].

Besides direct measurements, indirect methods have been established for obtaining the optical properties of tissue. While accurate direct methods are limited to thin samples, indirect methods allow samples with larger thicknesses [10]. These methods estimate the optical properties from the macroscopic measurements of diffuse reflection (DR), diffuse transmission (DT), total reflection (TR), total transmission (TT) and CT with the help of a light propagation model. In both cases, a fit of the data or an iterative procedure is required to derive the optical properties [7,11]. Especially two models have shown to produce accurate results: the analytic model of inverse adding doubling (IAD) [10,12] and inverse Monte-Carlo simulations (IMC) [7,11,13,14].

DR and DT measurements can either be done separately using a single integrating sphere or simultaneously by double integrating sphere measurements. Especially for thick samples it is likely to capture scattered photons during measurements of the collimated transmission CT using an integrating sphere system [15]. This leads to an overestimation of CT and an underestimation of the extinction coefficient ($\mu_t = \mu_a + \mu_s$) derived by the IAD technique [12] where μ_a is the absorption coefficient and μ_s the scattering coefficient. Separating the unscattered from the scattered photon can be quite hard. A possibility is to place the detector for CT in a distance from the sphere [16]. Still problems arise for strong scattering material as a significant fraction of the diffusely transmitted light leaves the sample close to the perpendicular of the surface and, therefore might reach the detector, leading to an overestimation of the CT.

To solve this problem with CT, some approaches were tested to bypass the error-prone measurement of CT. In general, these approaches are based on substituting the measurement of CT by the measurement of DT with the help of IMC. On the one hand, Bashkatov et al. [17] calculated the g-factor with fixed reduced scattering coefficient with the help of DT. On the other hand, the approach from Friebel et al. [18] uses the same measurement in combination with the Reynolds-McCormick phase function. Both methods seem to have a strong cross talk in the reconstruction between absorption and scattering which was shown by Terada et al. [11] and which we also saw in our previous studies [19]. Most likely this is caused by the effect that the back reflection for high absorption is no Lambertian reflector any more [7].

Another factor which should be considered is the tissue preparation. In general, fresh tissue or even in-vivo tissue is preferred. Often tissue has to be homogenized. This might lead to errors as it was shown that freezing and grinding procedures can alter the optical properties strongly [20]. For the absorption coefficient, this effect occurs due to fact that for homogenized tissue, the absorber is equally distributed instead packed in specific areas (e.g blood in blood vessels). Hence, light interacts more often with the absorber. Therefore, the effect of the absorber is stronger [21].

Due to alterations of the sample, the final goal is in-vivo measurements. As indirect methods do not require thin tissue samples, it is possibly to estimate the optical properties from in vivo measurements. In vivo techniques include methods measuring the steady-state diffusion-

Biomedical Optics EXPRESS

reflection-spectroscopy (DRS). The spatially-resolved steady-state local DRS can be measured by using illumination and multiple detection fibres in contact with the tissue surface. The detection fibres are located in different radial distances from the source fibres and measure the local DR as a function of the radial distance. For this, a model is required such as done by empirical models by Perelman et al. [22] which got extented by Zonios et al. [23]. However, these models are fairly complicated and show strong systematic errors in the measured optical properties. For this reason, Zonios et al. [24] suggested a new and simple model in which the geometry of the detector is calibrated by measuring a few known samples. Afterwards, it can be used with much lower errors of the reconstructed optical properties as the two previous models. In conclusion, the optical properties can be reconstructed fairly well. Other models rely on diffusion theory [25]. However, certain source-detector distances and a priori known parameters are required [25]. Another spatially-resolving approach uses absolute reflectance measurements as input to a neural network trained with MC data to estimate the optical properties [26]. A further alternative was presented by a study from Bargo et al. [27], in which an empirical light transport model was used. Nevertheless, all these approaches have the downside to only measure the absorption coefficient and the reduced scattering coefficient ($\mu_s' = \mu_s \cdot (1 - g)$) where g is the anisotropy factor.

Besides spatially-resolved steady-state diffuse reflectance measurements, source-detector fibre pairs can also be used for time-resolved measurements of the diffuse reflectance. In time-domain measurements sample tissue is probed by a short laser pulse and the resulting temporal broadening, caused by the propagation through the tissue, is measured [28]. Again a diffusion approximation model can be used to derive the optical properties. This method is limited to low absorbing regions of the wavelength due to the limits of the diffusion approximation model and a low degree of broadening, leading to low signal, in the highly absorbing regions [28]. Frequency-domain measurements can be conducted by illuminating laser beams and detecting the amplitude modulation and phase shift of the transmitted or reflected photon density [29,30]. However, the necessary technology to generate short enough light pulses for the time-resolved and frequency-domain techniques come with high costs and complex implementation compared to the steady-state methods [31].

As already mentioned, the main drawback of the indirect methods, which include the in vivo methods, lies in their dependence on a light propagation model. Considering especially the IMC technique errors can not only occur within the measurements but also within the data processing. In IMC simulations a phase function is used to estimate the optical properties. It has been shown that the phase function used in simulation has a strong effect on the results [32,33]. Especially the scattering coefficient μ_s showed an extremely sensitive response to the shape of the phase function [34]. Therefore, choosing the appropriate phase function for the set-up and the sample is crucial. With the example of whole blood, it was shown that the optimal phase function is highly dependent on the sample [14].

Referring to blood, it was shown that the scattering phase function of a single red blood cell cannot be applied to whole blood as interference of waves scattered by neighbouring cells needs to be considered in the phase function. Otherwise no accurate results for the optical properties can be obtained as a broadening of the scattering characteristics is associated with the interference [14]. If such effects and characteristics of the sample are not known a priori and considered in the simulation, the estimated properties might be erroneous. Especially for tissues including inhomogeneities it is difficult to determine the phase function. In this case mostly experimental measurements on thin tissue samples need to be conducted to obtain the phase function which involves a certain amount of effort. On the other hand, assumptions in the phase function can be critical as it has been shown that not considering the alteration of the reflectance angles as a function of the absorption coefficient leads to strong errors of estimating the optical properties [7,35].

Biomedical Optics EXPRESS

Due to the mentioned limits and drawbacks of the indirect methods combining macroscopic measurements with inverse light propagation models, other approaches should be verified and understood better. In a recent work of our group, a set-up was presented for measuring the collimated transmission CT by collimating the beam after passing through the sample without further assumptions on the light propagation [19]. With this set-up there was still an overlap between the collimated transmission CT and diffuse transmission DT. To overcome this issue in this work, a 4f set-up is presented and evaluated that makes use of optical Fourier transformation to separate CT and DT. Furthermore, it is proven in this study that CT and DT do not overlap significantly with a 4f set-up for a wide spectral range despite chromatic aberrations of the lenses. A mathematical model is presented which allows the derivation of the CT for the whole spectra with a few rather cheap laser diodes. The theoretical model is derived once from the diffusion approximation as commonly known equations are used and once from a more general approach. Both derivations show the same results. Moreover, it is shown experimentally that the derived formulas work outside the range of diffusion approximation as predicted by the more general approach. Finally, it is shown that the model can be used to derive the scattering coefficient μ_s directly without the use of any inverse simulation method such as IAD and IMC.

2. Theoretical considerations

The goal of the theoretical considerations is to derive a model which can describe the relationship between CT and TT. Thereby, the ansatz is to describe the ratio of TT and CT instead of both single quantities. Thereby two approaches are presented. The first approach is based on well known diffusion approximations with a new way of recombining them. For this, a nearly non-absorbing media as in the diffusion approximation is assumed. To compensate for this approximation, an error term is added of the approximations and to derive more general results again. The second approach shows that the same result can be derived by a more general approach. Both approaches are presented as it might provide some insight or helpful summary for readers with interest on the theoretical aspects.

2.1. Low absorption approximation

In general, the CT can be described by the following Beer-Lambert law:

$$CT = e^{-(\mu_a+\mu_s)\cdot d} \tag{1}$$

where μ_a is the absorption coefficient, μ_s the scattering coefficient and d the thickness of the sample. The diffuse transmission (DT) can be approximated for thick materials with high scattering and low absorption with Eq. (2) derived from the diffusion approximation where $3\mu_a(\mu_a + \mu_s \cdot (1-g)))^{\frac{1}{2}} \cdot d$ is taken from the diffusion approximation. It should be noted that for thinner samples, Eq. (2) will overestimate the transmission. For practical reasons, the discrepancy can be put into an error term $(E(\mu_a, \mu_s, \langle d\rangle))$ in the exponent. The dependence of E from $\langle d\rangle$ describes also other effects which are relevant in practical measurements. For example, a model of a turbid slab can be assumed. However in practice, the sample size cannot be infinite to the side as shown in Fig. 1. Thus, light will leave the sample in x and y direction. This depends on μ_a, μ_s, and the geometry.

$$DT = e^{-(3\mu_a(\mu_a+\mu_s\cdot(1-g)))^{\frac{1}{2}}\cdot d - E(\mu_a,\mu_s,\langle d\rangle)} \tag{2}$$

In Eq. (2), g is the anisotropy factor and $(E(\mu_a, \mu_s, \langle d\rangle))$ in the exponent the error term. The error term depends on the mean distance $\langle d\rangle$ the light travels, the scattering coefficient and the absorption coefficient.

Biomedical Optics EXPRESS

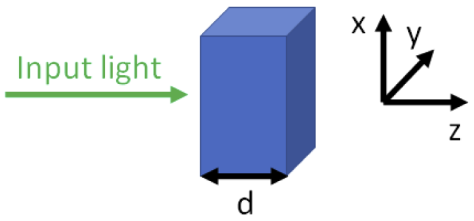

Fig. 1. If the light comes from the left, along the z-axis, there will be the reflection towards negative z and the transmission towards positive z. Additionally, in practical experiments light will leave the sample in x and y direction.

To derive a single parameter, the ratio factor k is introduced as follows:

$$k = \frac{TT}{CT} \tag{3}$$

Using TT instead of DT has the advantage that TT can be measured easily with high precision with an integration sphere set-up. Due to the fact that for thick samples the DT is nearly equal to TT as CT is very small, TT is replaced by DT:

$$k = \frac{TT}{CT} \approx \frac{DT}{CT} = e^{-(3\mu_a(\mu_a+\mu_s\cdot(1-g)))^{\frac{1}{2}}\cdot d+(\mu_a+\mu_s)\cdot d-E(\mu_a,\mu_s,\langle d\rangle)} \tag{4}$$

For all further calculations, the k-value will only be defined by dividing TT by CT due to simplifications of the experimental conditions even if the earlier set approximations are not valid:

$$k = \frac{TT}{CT} = e^{-(3\mu_a(\mu_a+\mu_s\cdot(1-g)))^{\frac{1}{2}}\cdot d+(\mu_a+\mu_s)\cdot d-E(\mu_a,\mu_s,\langle d\rangle)} \tag{5}$$

To simplify Eq. (3), a high scattering case is assumed:

$$\mu_a \ll \mu_s \tag{6}$$

Therefore, Eq. (5) becomes with Eq. (6) the following:

$$k = e^{-(3\mu_a(\mu_s\cdot(1-g)))^{\frac{1}{2}}\cdot d+\mu_s\cdot d-E(\mu_a,\mu_s,\langle d\rangle)} \tag{7}$$

A second approximation can be done with Eq. (7) as $(\mu_a \cdot \mu_s)^{0.5} \ll \mu_s$. Therefore, k can be simplified to the following equation:

$$k = e^{\mu_s\cdot d-E(\mu_a,\mu_s,\langle d\rangle)} \tag{8}$$

In summary, the ratio between the total transmission and the collimated transmission is proportional to $e^{\mu_s\cdot d}$. This result is valid for the range of the diffusion regime. Furthermore, $E(\mu_a, \mu_s, \langle d\rangle)$ has to be bigger than zero due to the fact that normal scattering will be underestimated by using the k-value instead of the CT.

From Eq. (8) the scattering coefficient can be calculated:

$$\mu_s(\lambda) = \frac{\ln(k(\lambda)) + E(\mu_a(\lambda), \mu_s(\lambda), \langle d\rangle)}{d} \tag{9}$$

2.2. General solution

The general case tries to describe a solution outside the limitations of the diffusion approximation which was used in the last section. It should be noted that the approach is taken to find a

Biomedical Optics EXPRESS

plausible rough description which does not provide an exact description. To compensate this, all the unknown are put in an error term as in the previous section which should compensate the simplifications. For the general solution, the definition of DT from Eq. (2) is not valid due to the fact that with higher absorption the diffusion approximation is not valid any more. In general, for zero absorption and infinite thickness all the light has to be scattered. Hence theoretically, it can distribute to DT_{gen} reduced by the light which is absorbed along its path. Thereby, DT_{gen} is the diffuse transmission for the general solution.

$$DT_{gen} = \left(1 - e^{-\mu_s \cdot d}\right) \cdot e^{-\mu_a d} \tag{10}$$

As TT is required, CT is added to Eq. (10):

$$TT = \left(1 - e^{-\mu_s \cdot d}\right) \cdot e^{-\mu_a d} + e^{-(\mu_a+\mu_s)\cdot d} \tag{11}$$

Eq. (11) is overestimating TT as the term for DT is too large. Thus, an error term is added to Eq. (11) in the exponent:

$$TT = \left(\left(1 - e^{-\mu_s \cdot d}\right) \cdot e^{-\mu_a d} + e^{-(\mu_a+\mu_s)\cdot d}\right) \cdot e^{-E(\mu_a,\mu_s,\langle d\rangle)} \tag{12}$$

where $E(\mu_a, \mu_s, \langle d\rangle)$ is the error term. As TT is overestimated, $E(\mu_a, \mu_s, \langle d\rangle)$ has to be positive as in Eq. (8). Now, the k-value can be written as follows:

$$k = \frac{TT}{CT} = \left(\left(1 - e^{-\mu_s \cdot d}\right) \cdot e^{-\mu_a d} + e^{-(\mu_a+\mu_s)\cdot d}\right) \cdot e^{-E(\mu_a,\mu_s,\langle d\rangle)} \cdot e^{(\mu_a+\mu_s)\cdot d} \tag{13}$$

Eq. (13) can be rearranged:

$$k = \left(\left(1 - e^{-\mu_s \cdot d}\right) \cdot e^{\mu_s d} + 1\right) \cdot e^{-E(\mu_a,\mu_s,\langle d\rangle)} = e^{\mu_s \cdot d} \cdot e^{-E(\mu_a,\mu_s,\langle d\rangle)} \tag{14}$$

Eq. (14) is identical to Eq. (8). Thus, μ_s is the same as in Eq. (9):

$$\mu_s = \frac{\ln(k) + E(\mu_a, \mu_s, \langle d\rangle)}{d} \tag{15}$$

2.3. Discussion of the theoretical considerations

As a general consideration for $\mu_a \gg \mu_s$ or better $\mu_s \to 0$ (Beer-Lambert regime), all the scattered light has to be absorbed quickly and, therefore, $TT \approx CT$ is valid. Hence, k is one. Plugging this into Eq. (15), leads to $\mu_s = 0$. Hence in the Beer-Lambert regime, the error term from Eq. (15) becomes zero. In general, it should also be considered that k is a function of the wavelength as the scattering coefficient is a function of the wavelength and, therefore, Eq. (15) becomes the following:

$$\mu_s(\lambda) = \frac{\ln(k(\lambda)) + E(\mu_a(\lambda), \mu_s(\lambda), \langle d\rangle)}{d} \tag{16}$$

Equation (16) shows the two advantages of this ansatz to use the ratio of TT and CT to derive the scattering coefficient. First, a direct and easy calculation can be used to derive the scattering coefficient if the error term can be ignored or is known. This also leads to the implication that TT and CT are proportional to each other. Second in contrast to the calibration step, any errors for the calculation/measurement of k have only a logarithmic effect on the resulting scattering coefficient. Therefore, miscalculations of a factor of two or more will lead to only minimal changes of the results. Hence, it is expected that this method will provide robust results. Finally, the effect of the error term can be derived by comparison to literature or better the measurement with the collimated transmission. Therefore, this method also provides a simple mean of evaluating it.

Biomedical Optics EXPRESS

3. Experimental validation

3.1. Set-up

For measuring the collimated transmission, the set-up consist of four lasers: 632 nm HeNe Laser (Thorlabs HNL225R), 450 nm diode laser (RLDD450-40-5, Roithner LaserTechnik GmbH, Austria), 808 nm diode laser (RLDB808-120-3, Roithner LaserTechnik GmbH, Austria), 980 nm diode laser (RLDB980-120-3, Roithner LaserTechnik GmbH, Austria) and a 4f-filter as shown in Fig. 2. The advantage of using an optical Fourier transform is that the DT and CT can be separated easily. The aperture after the cuvette and the aperture with a distance of 4f behind the cuvette placed in the holder will filter out all the light which is not originated within the beam diameter. The aperture with a distance of 2f will filter out effectively all the light which has a different direction than the collimated beam. By doing so, also the slightly scattered light which would pass through a normal aperture set-up can be filtered out.

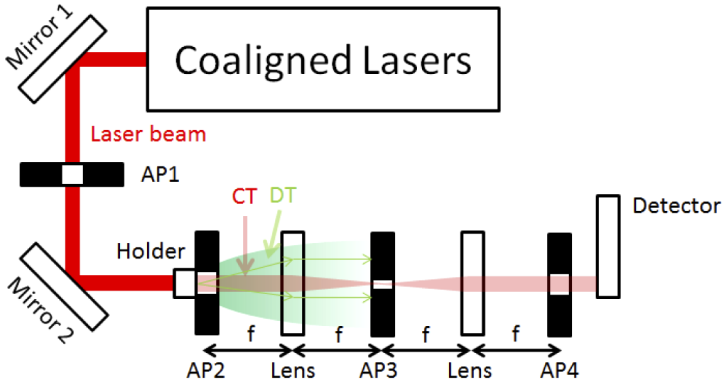

Fig. 2. The set-up for measuring the collimated transmission: A HeNe laser and three laser diodes are guided into the 4f-filter by two mirrors. The 4f-filter consists of the lenses and three apertures for filtering. The cuvette for measuring is added in the holder.

The laser is guided with two mirrors into the 4f-filter. These two mirrors are used to make the set-up more compact and they allow an easier alignment of the beam on the optical axis of the 4f-filter. Between both mirrors, there is an aperture (AP1) for giving the laser beam a round shape due to the fact that the laser beams from the diode lasers are elliptical. After this, the beams pass the holder for the sample. Directly behind that, there is the second aperture (AP2) to filter out the light which does not belong to the original laser beam. In a distance of 75 mm behind the sample there is a lens with a focal length of 75 mm. In its second focus, there is the third aperture (AP3) to filter out the spatial frequencies which do not belong to the collimated laser (CT). Hence, AP3 is the essential part of this set-up to improve the filtering out of the DT. Due to the fact that AP3 is in the Fourier plane, every light can be removed which does not have the same direction as the coaligned lasers. In a distance of further 75 mm there is another lens with a focal length of 75 mm. In its second focal point there is a further aperture (AP4) to filter out light not originating from the original beam. By using this 4f-filtering, the effective filtering can be ensured.

In theory, AP2 and AP4 should filter out the same light and therefore only one of these two filter would be required. However, the usage of both apertures improves the results of the measurement of the collimated transmission. Most likely small misalignments might be compensated by the usage of both apertures. Finally, the power of the laser beam is measured behind the fourth aperture with a diode based power meter (S130C, Thorlabs, USA). The laser power is measured with and without the sample for each measurement to compensate power fluctuations of the laser.

Biomedical Optics EXPRESS

For the measurements of TT, a spectrophotometer (Shimadzu UV-3600 UV-VIS-NIR, Japan) is used. It is the same system as in our previous study [19] with the change that instead of the integration sphere ISR-3100 the integration sphere LISR-3100 is used. The LISR-3100 is a larger version of the ISR-3100. The diameter of the integration sphere is 16 cm.

3.2. Experimental parameters

Before any of the theoretical considerations can be proven, it has to be proven that the set-up in Fig. 2 can measure the CT correctly. Therefore, four different intra-lipid solutions (IL, Fresenius Kabi AB, Sweden) are filled in a 1 cm thick cuvette with a height of 4 cm (Fluorescence cuvette, Hellma, Germany). The used IL concentrations are 0.05 %, 0.1 % and 0.2 %. This leads to a mean free path of the scattering of 0.045 cm to 3.4 cm for the used wavelengths in this study according to Aernouts et al. [36]. For each concentration and wavelength, the CT and TT are measured. From these, the k-value and the scattering coefficient are derived.

For the CT, it is shown that Beer-Lambert law is followed and, therefore, there is no overlap between CT and DT in the measurement. Moreover, the resulting scattering coefficients are compared to Aernouts et al. [36]. They measured the optical properties with help of the standard integration sphere set-up with a very high precision with the help of an inverse Monte-Carlo algorithm. For illumination, they use a super continuum laser.

Afterwards, the effect of the error function is tested. As the theory predicts, in the diffuse regime, the results should be valid. For the absorption regime the absolute error might go to zero. However, the relative error might still be high. To evaluate the error, a single scattering concentration of IL with 0.1 % is used and blue ink is added in different concentrations. The blue ink is Pelikan 4001 Royal Blue Ink (Pelikan Holding AG, Schindellegi, Switzerland). The concentration is varied from 1:50 to 1:5000. For the high concentrations of ink, the absorption is clearly dominating while for the low concentrations the scattering is still dominating. The values for the absorption coefficient of the ink are measured by a spectrophotometer (Shimadzu UV-3600 UV-VIS-NIR, Japan)

Moreover, it should be considered that the measured TT depends on the cuvette size. To estimate the difference between the measured TT and the real one, a Monte Carlo simulation (MCS) is done. The MCS is done with help of MCX [37,38] for a wide range of the scattering and absorption coefficients. In total, 10 different μ_a and μ_s spanning over the range of relevant optical properties are simulated, leading to 100 parameter combinations. The g-factor is set to 0.6. In total, two different set-ups are simulated: First, a cuvette including the glass boundaries with a dimension of 4 cm, 1cm and 1 cm in x,y and z direction is simulated according to Fig. 1 which is the same as used in the experiments. For the second MCS set-up, the size in x and y direction is increase to 10 cm without a glass boundary in x and y direction. The correction factor is derived by dividing TT from both set-ups. The results for the correction factor are either fitted by a polynome (low absorption) or interpolated by cubic fitting (python, scipy: interpolate.interp2d). From the fit or the interpolation, the required correction factors are taken. An example for low absorption is shown in the attachments.

3.3. Validation of the set-up

CT The validation is done by testing Lamberts law and verifying that CT can be reconstructed for not measured IL concentrations. For simplification, this is done for the IL concentration of 0 %. Fig. 3 shows the dependence of the logarithmic CT on IL concentrations for 450 nm, 632 nm, 808 nm and 980 nm and the corresponding linear fits. It can be seen that there is a perfect exponential decay of the CT as a function of the concentration as predicted by Lamberts law. It should be noted that it is only valid for CT. Nevertheless, Lamberts law depends on the scattering and absorption coefficient instead of depending on the absorption coefficient alone: $I = I_0 \cdot e^{-(\mu_a+\mu_s)\cdot d}$. As for IL, the absorption coefficient is nearly zero, the resulting CT only depends on the scattering

Biomedical Optics EXPRESS

coefficient. Therefore, there is an exponential decay for CT as the function of the IL concentration. The scattering coefficient decreases for increasing wavelengths. This is true for scattering in the Rayleigh-regime, in the Mie-regime and in the geometrical-scattering-regime. Hence, the decay is stronger for shorter wavelengths. All fits in Fig. 3 have an R^2-value larger than 0.99. Nevertheless, the measurement value of an IL concentration of 0.2 % shows an error for the measurement at 450 nm as the detector cannot resolve the low power. This result allows two conclusions. First, the 4f set-up works. Second, the mixing process of the IL has no obvious errors.

Nevertheless, there might still be an offset with the data. To check this, the intersection with the y-axis and therefore the theoretical transmission without IL is shown in Table 1.

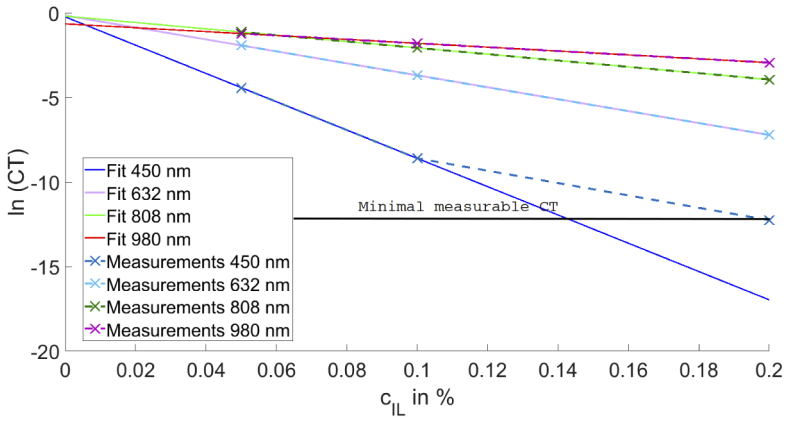

Fig. 3. Concentration dependence of the logarithmic CT for 450 nm, 632 nm, 808 nm and 980 nm and the corresponding fits. The R^2 value is in all cases larger than 0.99. The CT-value for 0.2 % IL-concentration for 450 *nm* is not included for the fit as the detector cannot measure the real value.

Table 1. Estimated transmission (intersection point of fit with y-axis) without IL derived from the fits in Fig. 3 and comparison to the direct measurements of CT and TT for a water filled cuvette.

Wavelength in nm	450	632	808	980
Estimated transmission without IL	80 %	86 %	83 %	53 %
Measured transmission water (TT)	88 %	88 %	87 %	56 %
Measured transmission water (CT)	86 %	89 %	85 %	53 %

In Table 1 it can be seen that the predicted results for 0 % IL are realistic. However, there are small inconsistencies in Table 1 for TT and CT which might be caused by a not perfectly linear behaviour of the detectors being used for measuring CT and TT or by small non repeatable power fluctuations of the laser. In all cases, the fits in Fig. 3 are used to estimate the transmission for an IL concentration of 0 %. Therefore, the set-up measures the CT correctly also for different wavelengths despite the chromatic aberrations of the lenses.

In general, the manufacturing of the right IL concentration has to be very precise. Tiny errors show huge effects on the measured CT as these errors are in the exponent of the Lamberts law function. Despite the fact that errors from the mixing process provide an exponential scaling of the resulting error for the CT, there is no significant error found. Furthermore, the slightly lower transmission might also be caused by minimal amounts of dust on the cuvettes or sticking of a tiny amount of oil from the IL on the cuvette surface in a different way than an air-IL surface.

Biomedical Optics EXPRESS

However, the resulting error of the estimated CT for a water filled cuvette is less than 10 % which is a very good result. Moreover, the drop of the CT and TT for 980 nm is found as it is caused by the absorption of the water. Hence, the set-up provides excellent measurements of the collimated transmission. In summary, it can be concluded that the final measuring errors should be below the error from the intersection with the y-axis. Therefore, they should be below 10 %.

3.4. Result of μ_s

Table 2 provides an overview of the different sources of the scattering coefficient used in this and the next section. Thereby, μ_{s_k} is the scattering coefficient derived from the k-value from Eq. (16). The scattering coefficient $\mu_{s_{CT}}$ is calculated by Lambert law from the collimated transmission and $\mu_{s_{Aernouts}}$ is the scattering coefficient calculated by the equations provided by Aernouts et al. [36].

Table 2. Overview of different scattering coefficients.

Scattering coefficient	Derived by/from
μ_{s_k}	k-value from Eq. (16)
$\mu_{s_{CT}}$	Lambert law with CT
$\mu_{s_{Aernouts}}$	Aernouts et al. [36]

Figure 4 shows μ_{s_k}, according to Eq. (16), the scattering coefficient as a function of the wavelength or different IL-concentrations. On the left side, the uncorrected results are shown. On the right side, the results are shown with the correction for finite cuvette sizes (Correction for TT). For all cases, the higher the concentration of IL is, the higher is μ_{s_k}. The same trend is found for the wavelength: the shorter the wavelength, the higher μ_{s_k}. The value for an IL concentration of 0.2 % and 450 *nm* is too low and underestimated due to the fact that the real CT cannot be measured correctly as shown on Fig. 3. It can be seen that the correction for the underestimated TT due to its finite cuvette size with the correction factor from the MCS leads to a strong increase of μ_{s_k} especially for low values of μ_{s_k}. Overall, the corrected values seem to be more realistic.

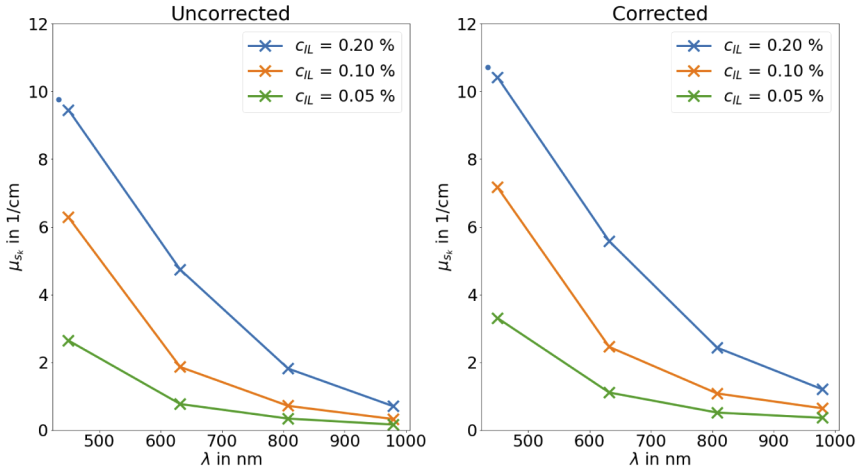

Fig. 4. The derived scattering coefficient μ_{s_k} as function of the wavelength without (left) and with (right) the correction of TT due to its finite cuvette size with the correction factor from the MCS. The value marked by the point is the value for 0.2 % IL concentration at 450 nm which has a too high measured CT and therefore a too low scattering coefficient.

The values of the scattering coefficient derived by the k-value (μ_{s_k}) in comparison to the direct measurement ($\mu_{s_{CT}}$, left) and with Aernouts et al. [36] (right) are shown in Fig. 5. The upper

Biomedical Optics EXPRESS

graphs show the results without correction of TT and the lower ones show the results with the correction for TT. Overall, it can be seen that the results measured with the presented method in this study are fairly linear compared to the measurements from Aernouts et al. [36] and to $\mu_{s_{CT}}$. The agreement is higher with the results derived from CT. In this case, around 99 % of the variance can be explained by the linear fit. The value for 0.2 % IL for 450 nm is present and agrees with the linearity to $\mu_{s_{CT}}$. The measuring error does not influence this as both values are altered by the same amount. For the comparison to $\mu_{s_{Aernouts}}$, the discrepancy gets larger. Nevertheless, it should be noted that $\mu_{s_{Aernouts}}$ for 450 nm can only by estimated from Aernouts et al. [36] due to the fact that it is outside their measuring range. Hence, only hints can be derived from this. Moreover, it should be noted that the g-factor varies from 0.8 at around 550 nm to 0.6 at around 1000 nm [36]. These differences in the g-factor do not seem to influence the results shown in Fig. 5.

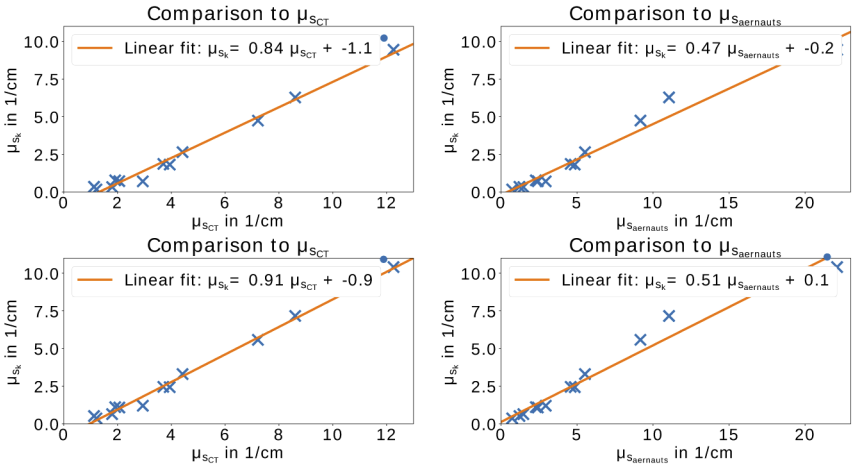

Fig. 5. Comparison of μ_{s_k} to $\mu_{s_{CT}}$ (left) and $\mu_{s_{Aernouts}}$ (right). In both graphs, the blue crosses represent the values from μ_{s_k} over the corresponding scattering coefficient. The lower graphs represents the results with the correction of TT for the used finite cuvette. All fits explain most of the variance (R^2>0.96). The value marked by the point is the value for 0.2 % IL concentration at 450 nm which has a too high measured CT and, therefore, a too low scattering coefficient (μ_{s_k} and $\mu_{s_{CT}}$).

For low scattering, μ_{s_k} underestimates the real scattering stronger than for high scattering due to a present offset. Nevertheless, it can be concluded that the proportionality of $\frac{TT}{CT}$ to $e^{\mu_s \cdot d}$ is true. Moreover, the correction of TT seems to improve the relationship between μ_{s_k} and $\mu_{s_{CT}}$ as well as $\mu_{s_{Aernouts}}$. In comparison to the results from $\mu_{s_{CT}}$, there is still an offset of around $\frac{1}{cm}$. Thus, the error term ($E(\mu_a, \mu_s, \langle d \rangle)$) has a constant term of $\frac{1}{d}$.

In general, there is a significant difference to the results from Aernouts et al. [36] and the results derived with CT. The discrepancy between the results from Aernouts et al. [36] and the results derived with CT might be explained as follows: First, the IL from (IL, Fresenius Kabi AB, Sweden) might show a stronger batch to batch variation then it is expected from before [39]. Second, in at least one of the measurements from either this study or the one from Aernouts et al. [36], there is a systematic error for the calculation of the scattering coefficient. Most likely, the discrepancy is caused by the latter. Due to fact that Aernouts et al. [36] did measure down to 0.227 % IL-concentration while these values are extrapolated to much lower concentrations in this study. By this, the results for these low concentrations might be flawed. Moreover, the values for 450 nm are outside their measuring range from Aernouts et al. [36]. The second error is caused by the fitting function. The fitting function $\mu_s = a \cdot \lambda^{-b}$ was used by Aernouts et al.

Biomedical Optics EXPRESS

[36]. However this function is numerically unstable as the fitting parameter might converge for different starting conditions to different values. This might lead to the fitting parameter a to vary over many orders of magnitude with the same data. This issue can be easily overcome by changing the function to $\mu_s = 10^a \cdot \lambda^{-b}$ as we stated this solution already in an older study [40]. Hence, while the results are in certain agreement to Aernouts et al. [36], the comparison to $\mu_{s_{CT}}$ is much more suitable.

3.5. Experimental effect of all correction factors with dependence on μ_a

In this section, it is shown how the correction of TT and the correction of TT plus the found value from the error term $E(\mu_a, \mu_s, \langle d \rangle) = \frac{1}{d}$ influence the scattering coefficient. First, the effect of the correction of TT is presented with focus on the effect of the absorption coefficient. Afterwards, the effect of the correction of TT and the effect of the error term are presented to show that the scattering coefficient can be clearly measured with small errors.

Figure 6 shows the effect of the absorber on μ_{s_k} for 0.1 % IL for different wavelengths over the ratio from μ_a and $\mu_{s_{CT}}$ (relative absorption). The results for 980 nm are not shown due to the increased absorption from water. On the left side, the results are shown without any correction while on the right side, the results are shown with the correction of TT. In both cases, the absorption coefficient has some influence. The increasing discrepancy for lower μ_{s_k} can be explained by the constant offset between μ_{s_k} and $\mu_{s_{CT}}$ which leads to stronger errors for lower scattering coefficients. In summary, the expectations of the model to be able to measure the scattering coefficient can be fulfilled with limitations.

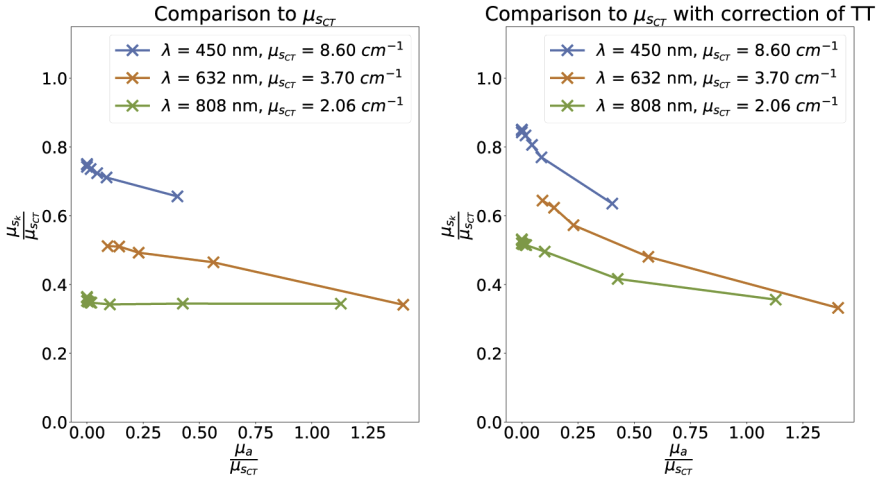

Fig. 6. Effect of the absorption coefficient on the ratio from μ_{s_k} to $\mu_{s_{CT}}$ for an IL concentration of 0.1 %. On the left side, normal formula is used and on the right side the correction of TT is applied.

Figure 7 shows the effect of the absorber on the derived scattering coefficient and, thus, summarizes all results. On the left side, the ratio from μ_{s_k} and $\mu_{s_{CT}}$ is shown over the wavelength for different IL concentrations. On the right side, the same ratio is shown for 0.1 % IL over the ratio from μ_a and $\mu_{s_{CT}}$ (relative absorption). On the top, results are shown with the correction by the error term ($E(\mu_a, \mu_s, \langle d \rangle) = \frac{1}{d}$). On the bottom, the results are shown inclusive the error term ($E(\mu_a, \mu_s, \langle d \rangle) = \frac{1}{d}$) and the corrections for TT. With all corrections the error for μ_{s_k} is less than 25 %. The results presented here, show the validity of the approach and the results are in agreement to the predictions. Up to around $\mu_a \approx \mu_s/2$, the effect of the absorption is rather small despite the fact that there is a clear influence. It can be seen that for low scattering both

Biomedical Optics EXPRESS

corrections improve the values for μ_{s_k}. However, the effect of the absorption coefficient on μ_{s_k} is compensated by the measurement with a cuvette with a small size. In this case, the TT correction factor decreases for increasing absorption coefficients. In summary with all corrections, the discrepancy is around 20 % for wide range of μ_s and μ_a and the final error by the usage of the k-value instead of CT is only a constant.

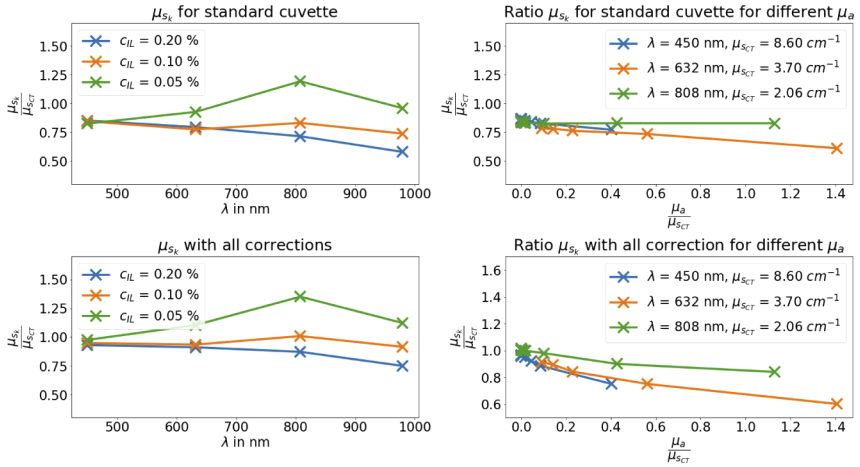

Fig. 7. Effect of the corrections by the constant error term ($E(\mu_a, \mu_s, \langle d \rangle)$) with the value $E(\mu_a, \mu_s, \langle d \rangle) = \frac{1}{d}$ (top) and the correction from the error term plus the correction from TT (bottom).

4. Discussion and conclusion

This study could show that CT and TT are proportional to each other with the proportionality constant e^{μ_s}. Hence, the scattering coefficient can be reconstructed by this. As the absorption coefficient influences CT and TT, the overall influence is reduced on the ratio of both them. Therefore, the absorption coefficient shows a lower influence on the reconstructed scattering coefficient. In conclusion, it is possible to measure the scattering coefficient directly even for absorbing media without any inverse algorithm such as IAD or IMCS. Moreover, the measurement errors are fairly low due to the fact that all measurements and, therefore, the errors have only a logarithmic dependence.

The most interesting result is that there seems to be a fixed ratio k between CT and TT as shown in Eq. (3) or 13. The ratio is proportional to $k \propto e^{\mu_s}$. Nevertheless, it is only true in practice if the size of the sample is larger than the mean free scattering path. Experimentally, it is also helpful if the thickness of the sample is lower than its other dimensions. However, this was not tested in this study. There are only indirect results pinpointing in this direction. Furthermore, it is not tested if the found relationship between CT and TT is true for very strong scattering samples which are larger than 15 times the mean free path. Thus, these effects should be investigated in later studies. Potentially, the geometry can get linked with the mean path $\langle d \rangle$ which is neglected in this study. To be able to investigate a large variety of optical properties and sample geometries, a Monte-Carlo-simulation is proposed.

Combining the theoretical results with the experimental validation shows that TT and CT behave similar enough over a wide range of absorbing coefficients and scattering coefficients up to $\mu_a \leq \mu_s/2$ to allow a robust direct calculation of the scattering coefficient even in partly absorbing states. Nevertheless, it should be noted again that the proportionality of $\frac{TT}{CT}$ to $e^{\mu_s \cdot d}$ is

Biomedical Optics EXPRESS

only true if the mean free path is smaller than the dimensions of the sample. The description with the error term is valid as it leads to more exact results. In summary, the following is known:

- The error term is positive.
- The error term seems to be only dependent on d for low absorption ($\mu_s \gg \mu_a$).
- The error term increases for an increasing absorption coefficient. However, it might drop for strongly absorption dominated regimes.

TT, CT and the scattering coefficient can be seen as clearly linked to each other for the case of relatively low absorption. This might simplify the measurement of the scattering coefficient as it is done in this study or it might allow the characterization of CT for thick known samples with the help of measuring TT. Moreover, the results seems to be valid for different g-factors. According to Aernouts et al. [36], the g-factor varies from 0.8 at around 550 nm to 0.6 at around 1000 nm in IL. In this study, there is no wavelength dependent effect seen. Hence, the effect of the g-factor is expected to be neglectable. Thus, everything pinpoints that the results seem to be generalizable.

Funding

Deutsche Forschungsgemeinschaft (337270237).

Acknowledgement

The authors would like to thank the German Research Foundation (DFG-Deutsche Forschungsgemeinschaft) for its support. This work was achieved in the context of the DFG-project "Dreidimensionale Abbildung trüber Medien mittels hyperspektraler Bildgebung" (project number 337270237).

The authors gratefully acknowledge the funding of the Erlangen Graduate School in Advanced Optical Technologies (SAOT) by the Deutsche Forschungsgemeinschaft (German Research Foundation - DFG) within the framework of the Initiative for Excellence.

Disclosures

The authors declare no competing interests.

See Supplement 1 for supporting content.

References

1. L. Jones, N. Preyer, H. Wolfsen, D. Reynolds, M. Davis, and M. Wallace, "Monte carlo model of stricture formation in photodynamic therapy of normal pig esophagus," Photochem. Photobiol. **85**(1), 341–346 (2009).
2. L. Jones, N. Preyer Jr, M. Davis, C. Grimes, K. Edling, N. Holdgate, H. Wolfsen, and M. Wallace, "Light dosimetry calculations for esophageal photodynamic therapy using porfimer sodium," Proc. SPIE **6139**, 61391D (2006).
3. E. V. Salomatina, B. Jiang, J. Novak, and A. N. Yaroslavsky, "Optical properties of normal and cancerous human skin in the visible and near-infrared spectral range," J. Biomed. Opt. **11**(6), 064026 (2006).
4. T. L. Troy, D. L. Page, and E. M. Sevick-Muraca, "Optical properties of normal and diseased breast tissues: prognosis for optical mammography," J. Biomed. Opt. **1**(3), 342–356 (1996).
5. B. Wilson, M. Patterson, and S. Flock, "Indirect versus direct techniques for the measurement of the optical properties of tissues," Photochem. Photobiol. **46**(5), 601–608 (1987).
6. S. Prahl, "Everything i think you should know about inverse adding-doubling," *Oregon Medical Laser Center, St. Vincent Hospital* pp. 1–74 (2011).
7. D. Fukutomi, K. Ishii, and K. Awazu, "Highly accurate scattering spectra of strongly absorbing samples obtained using an integrating sphere system by considering the angular distribution of diffusely reflected light," Lasers Med. Sci. **30**(4), 1335–1340 (2015).
8. M. Van Gemert, S. L. Jacques, H. Sterenborg, and W. Star, "Skin optics," IEEE Trans. Biomed. Eng. **36**(12), 1146–1154 (1989).

Biomedical Optics EXPRESS

9. S. Jacques, "Optical properties of biological tissues: a review," Phys. Med. Biol. **58**(11), R37–R61 (2013).
10. S. A. Prahl, M. J. van Gemert, and A. J. Welch, "Determining the optical properties of turbid media by using the adding–doubling method," Appl. Opt. **32**(4), 559–568 (1993).
11. T. Terada, T. Nanjo, N. Honda, K. Ishii, and K. Awazu, "Error analysis of tissue optical properties determined by double-integrating sphere system and inverse monte carlo method," in *SPIE BiOS*, (International Society for Optics and Photonics, 2011), p. 78971W.
12. S. Prahl, "Everything i think you should know about inverse adding-doubling,".
13. A. N. Yaroslavsky, I. V. Yaroslavsky, T. Goldbach, and H.-J. Schwarzmaier, "Different phase-function approximations to determine optical properties of blood: A comparison," in *Optical Diagnostics of Biological Fluids and Advanced Techniques in Analytical Cytology*, vol. 2982 (International Society for Optics and Photonics, 1997), pp. 324–330.
14. M. Hammer, A. N. Yaroslavsky, and D. Schweitzer, "A scattering phase function for blood with physiological haematocrit," Phys. Med. Biol. **46**(3), N65–N69 (2001).
15. L. Wang and S. L. Jacques, "Error estimation of measuring total interaction coefficients of turbid media using collimated light transmission," Phys. Med. Biol. **39**(12), 2349–2354 (1994).
16. J. W. Pickering, S. A. Prahl, N. Van Wieringen, J. F. Beek, H. J. Sterenborg, and M. J. Van Gemert, "Double-integrating-sphere system for measuring the optical properties of tissue," Appl. Opt. **32**(4), 399–410 (1993).
17. A. N. Bashkatov, E. A. Genina, V. I. Kochubey, A. A. Gavrilova, S. V. Kapralov, V. A. Grishaev, and V. V. Tuchin, "Optical properties of human stomach mucosa in the spectral range from 400 to 2000 nm: prognosis for gastroenterology," Med. Laser Appl. **22**(2), 95–104 (2007).
18. M. Friebel, A. Roggan, G. J. Müller, and M. C. Meinke, "Determination of optical properties of human blood in the spectral range 250 to 1100 nm using monte carlo simulations with hematocrit-dependent effective scattering phase functions," J. Biomed. Opt. **11**(3), 034021 (2006).
19. M. Hohmann, B. Lengenfelder, R. Kanawade, F. Klämpfl, A. Douplik, and H. Albrecht, "Measurement of optical properties of pig esophagus by using a modified spectrometer set-up," J. Biophotonics **11**(1), e201600187 (2018).
20. E. Chan, T. Menovsky, and A. J. Welch, "Effects of cryogenic grinding on soft-tissue optical properties," Appl. Opt. **35**(22), 4526–4532 (1996).
21. J. C. Finlay and T. H. Foster, "Effect of pigment packaging on diffuse reflectance spectroscopy of samples containing red blood cells," Opt. Lett. **29**(9), 965–967 (2004).
22. L. T. Perelman, V. Backman, M. Wallace, G. Zonios, R. Manoharan, A. Nusrat, S. Shields, M. Seiler, C. Lima, T. Hamano, I. Itzkan, J. Van Dam, J. M. Crawford, and M. S. Feld, "Observation of periodic fine structure in reflectance from biological tissue: a new technique for measuring nuclear size distribution," Phys. Rev. Lett. **80**(3), 627–630 (1998).
23. G. Zonios, L. T. Perelman, V. Backman, R. Manoharan, M. Fitzmaurice, J. Van Dam, and M. S. Feld, "Diffuse reflectance spectroscopy of human adenomatous colon polyps in vivo," Appl. Opt. **38**(31), 6628–6637 (1999).
24. G. Zonios and A. Dimou, "Modeling diffuse reflectance from semi-infinite turbid media: application to the study of skin optical properties," Opt. Express **14**(19), 8661–8674 (2006).
25. R. Doornbos, R. Lang, M. Aalders, F. Cross, and H. Sterenborg, "The determination of in vivo human tissue optical properties and absolute chromophore concentrations using spatially resolved steady-state diffuse reflectance spectroscopy," Phys. Med. Biol. **44**(4), 967–981 (1999).
26. A. Kienle, L. Lilge, M. S. Patterson, R. Hibst, R. Steiner, and B. C. Wilson, "Spatially resolved absolute diffuse reflectance measurements for noninvasive determination of the optical scattering and absorption coefficients of biological tissue," Appl. Opt. **35**(13), 2304–2314 (1996).
27. P. R. Bargo, S. A. Prahl, T. T. Goodell, R. Sleven, G. Koval, G. Blair, and S. L. Jacques, "In vivo determination of optical properties of normal and tumor tissue with white light reflectance and an empirical light transport model during endoscopy," J. Biomed. Opt. **10**(3), 034018 (2005).
28. T. Svensson, S. Andersson-Engels, M. Einarsdóttír, and K. Svanberg, "In vivo optical characterization of human prostate tissue using near-infrared time-resolved spectroscopy," J. Biomed. Opt. **12**(1), 014022 (2007).
29. A. E. Cerussi, V. W. Tanamai, D. Hsiang, J. Butler, R. S. Mehta, and B. J. Tromberg, "Diffuse optical spectroscopic imaging correlates with final pathological response in breast cancer neoadjuvant chemotherapy," Philos. Trans. R. Soc., A **369**(1955), 4512–4530 (2011).
30. S. Fantini, S. A. Walker, M. A. Franceschini, M. Kaschke, P. M. Schlag, and K. T. Moesta, "Assessment of the size, position, and optical properties of breast tumors in vivo by noninvasive optical methods," Appl. Opt. **37**(10), 1982–1989 (1998).
31. A. Kim and B. C. Wilson, "Measurement of ex vivo and in vivo tissue optical properties: methods and theories," in *Optical-Thermal Response of Laser-Irradiated Tissue*, (Springer, 2010), pp. 267–319.
32. J. R. Mourant, J. Boyer, A. H. Hielscher, and I. J. Bigio, "Influence of the scattering phase function on light transport measurements in turbid media performed with small source–detector separations," Opt. Lett. **21**(7), 546–548 (1996).
33. A. Kienle, F. K. Forster, and R. Hibst, "Influence of the phase function on determination of the optical properties of biological tissue by spatially resolved reflectance," Opt. Lett. **26**(20), 1571–1573 (2001).
34. A. N. Yaroslavsky, I. V. Yaroslavsky, T. Goldbach, and H.-J. Schwarzmaier, "Influence of the scattering phase function approximation on the optical properties of blood determined from the integrating sphere measurements," J. Biomed. Opt. **4**(1), 47–54 (1999).
35. D. Fukutomi, K. Ishii, and K. Awazu, "Determination of the scattering coefficient of biological tissue considering the wavelength and absorption dependence of the anisotropy factor," Opt. Rev. **23**(2), 291–298 (2016).

Biomedical Optics EXPRESS

36. B. Aernouts, E. Zamora-Rojas, R. Van Beers, R. Watté, L. Wang, M. Tsuta, J. Lammertyn, and W. Saeys, "Supercontinuum laser based optical characterization of intralipid® phantoms in the 500-2250 nm range," Opt. Express **21**(26), 32450–32467 (2013).
37. Q. Fang and D. A. Boas, "Monte carlo simulation of photon migration in 3d turbid media accelerated by graphics processing units," Opt. Express **17**(22), 20178–20190 (2009).
38. L. Yu, F. Nina-Paravecino, D. R. Kaeli, and Q. Fang, "Scalable and massively parallel monte carlo photon transport simulations for heterogeneous computing platforms," J. Biomed. Opt. **23**(1), 010504 (2018).
39. L. Spinelli, M. Botwicz, N. Zolek, M. Kacprzak, D. Milej, P. Sawosz, A. Liebert, U. Weigel, T. Durduran, F. Foschum, A. Kienle, F. Baribeau, S. Leclair, J.-P. Bouchard, I. Noiseux, P. Gallant, O. Mermut, A. Farina, A. Pifferi, A. Torricelli, R. Cubeddu, H.-C. Ho, M. Mazurenka, H. Wabnitz, K. Klauenberg, O. Bodnar, C. Elster, M. Bénazech-Lavoué, Y. Bérubé-Lauzière, F. Lesage, D. Khoptyar, A. A. Subash, S. Andersson-Engels, P. D. Ninni, F. Martelli, and G. Zaccanti, "Determination of reference values for optical properties of liquid phantoms based on intralipid and india ink," Biomed. Opt. Express **5**(7), 2037–2053 (2014).
40. L. Kreiß, M. Hohmann, F. Klämpfl, S. Schürmann, F. Dehghani, M. Schmidt, O. Friedrich, and L. Büchler, "Diffuse reflectance spectroscopy and raman spectroscopy for label-free molecular characterization and automated detection of human cartilage and subchondral bone," Sens. Actuators, B **301**, 127121 (2019).